Article

Development of Rotational Fixity Factors for Vibration Design of Cross-Laminated Timber Floors

Sigong Zhang [1], Jianhui Zhou [2], Jan Niederwestberg [1] and Ying Hei Chui [1,*]

[1] Department of Civil and Environmental Engineering, University of Alberta; sigong@ualberta.ca (S. Z.); jan.niederwestberg@ualberta.ca (J. N.); yhc@ualberta.ca (Y. H. C.)
[2] Integrated Wood Engineering, University of Northern British Columbia; jianhui.zhou@unbc.ca
* Correspondence: yhc@ualberta.ca

Abstract: As an emerging building solution, cross-laminated timber (CLT) floors have been increasingly used in mass timber construction. The current vibration design of CLT floors is conservative due to the assumption of simple support conditions in the floor-to-wall connections. It is noted that end fixity occurs as a result of clamping action at the ends, arising from the gravity load applied by the structure above the floor and by the mechanical fasteners. In this paper, the semi-rigid floor-to-wall connections are treated as elastically restrained edges against rotations to account for the effect of partial constraint. A rotational end-fixity factor was first defined to reflect the relative bending stiffness between CLT floors and elastic restraints at the edges. Then, for the design of vibration serviceability of CLT floors as per the Canadian Standard for Engineering Design in Wood (CSA O86), restraint coefficients were defined and their analytical expressions were derived for natural frequencies and the mid-span deflection under a concentrated load, respectively. In particular, a simplified formula of the restraint coefficient for the fundamental frequency was developed to assist engineers in practical design. At last, by comparing with reported experimental data, the proposed design formula showed excellent agreement with test results. In the end, the proposed end fixity factor with their corresponding restraint coefficients is recommended as an effective mechanics-based approach to account for the effect of end support conditions of CLT floors.

Keywords: Cross-laminated timber floors; End supports; End fixity factor; Vibration serviceability

1. Introduction

Since introduced in the 1990s, cross-laminated timber (CLT) has been gaining popularity in mid to high-rise residential buildings and non-residential construction in Europe and North America [1]. When deployed for prefabricated wall and floor panels, CLT offers many advantages and has become a viable alternative to steel and concrete. However, due to its relatively large stiffness-to-mass ratios and low inherent damping, the design of CLT floors can be governed by vibration serviceability [2]. Design parameters of a 1 kN static deflection and the fundamental natural frequency have been proven to provide excellent predictions of CLT floor vibration performance [1]. Thus, an accurate calculation of such parameters is critical in assessing CLT floor performance.

To-date, most CLT buildings are platform construction, in which each successive storey is built from the floor below it. Due to the gravity loads from higher storeys when walls are rested directly on the floors, and due to floor-to-wall fixtures, a degree of restraint is expected in CLT floor-to-wall connections [3]. It is well established in the literature that such restraints at in-situ conditions of CLT floors have a significant influence on their dynamic properties, as confirmed by previous investigations and reported in [4]. In particular, in-situ tests performed by Zimmer and Augustin [5] have shown tendencies toward increased frequencies due to partial clamping of the CLT panels at the supports by the load of superimposed storeys above and floor-to-wall fixtures. In this regard, the lower the storey of a given floor in the building is, the higher the load on the supports by walls and the load from storeys above will be, which results in higher stiffness of the floor and, therefore, natural

Preprints (www.preprints.org) | NOT PEER-REVIEWED | Posted: 4 October 2018 doi:10.20944/preprints201810.0071.v1

frequencies and lower deflections. However, existing design methods [1,6–8] often assume simple support conditions for calculating natural frequency and deflection. Such an assumption cannot describe the floor boundary conditions in reality, which results in overly conservative design decisions. Parametric studies conducted by Schultz and Johnson [9] have shown that the rotational restraints at the ends of the floor panels could likely reduce the thickness of floor panels by up to 35% when vibrations govern the design. Furthermore, numerical analyses performed in [3] have indicated that the maximum displacement can be reduced up to 79% by increasing the support rigidity and the fundamental frequency increased by 23% and 99% for semi-rigid and fully clamped support conditions, respectively. However, previous studies have been limited to experimental and numerical approaches, with no reliable analytical treatment. Consequently, no practical design formulae are available for considering the restraints of end supports.

Therefore, in the present study, analytical methods are developed to account for the effect of partial constraint by treating the semi-rigid floor-to-wall connections as elastically restrained edges against rotation. A new end-fixity factor is first introduced to reflect the rotational stiffness of end support relative to the bending stiffness of the CLT panel. Then, the analytical expressions for natural frequencies and deflection under a concentrated load were derived, and the corresponding restraint coefficients were defined. A simplified formula of the restraint coefficient for the fundamental frequency was developed to assist engineers in achieving practical design. Finally, the proposed design formula is validated by comparing with test results. Excellent agreements have been observed.

2. End-fixity factors

Traditionally, the rotational stiffness, R, is commonly defined to account for the effects of rotational restraints at the end of a beam. Although these constants are straightforward in analyses, they actually have little practical use in determining the flexibility at the ends, because they are not related to the flexural rigidity of a structure. It is difficult to answer the question “How large a rotational stiffness can represent zero flexibility (i.e., fully clamped ends) and how small a stiffness for infinite flexibility (i.e., simply supported ends)? [10]" On the other hand, a highly nonlinear relationship between the rotational stiffness and structural performance and properties is unfavorable in design practice. For instance, if the rotational stiffness at the ends is low, small increases in the restraint stiffness result in appreciable increases in the frequencies and decreases in the deflection of the beam. However, if the rotational stiffness at the ends is high, very significant changes in restraint stiffness may produce only very small changes in the frequencies and deflection. Such non-linear features cannot be improved by non-dimensional ratios of the restraint stiffness at the end to the beam flexural rigidity (i.e., R/EI) [11]. A similar issue was reported in the design of semi-rigid beam-column members in the steel-framed structures [12,13].

In this matter, a “fixity factor" was developed for semi-rigid beam-column members to characterise the relative stiffness between the member and the rotational spring of the end-connection, which was first proposed in [14] as

$$r = \frac{1}{1+3\dfrac{EI}{RL}} \tag{1}$$

in which R is the end-connection spring stiffness, EI is the flexural rigidity of the beam and L is the span as shown in Fig. 1. The physical meaning of the fixity factor, r, can be interpreted as the ratio of the end rotation α under a unit end moment divided by the rotation θ of the beam plus the connection spring, for the same unit end moment. From the illustration of Fig. 1, this factor can be derived as

$$r = \frac{\alpha}{\theta} = \frac{\alpha}{1/R+\alpha} = \frac{1}{1+3\dfrac{EI}{RL}} \tag{2}$$

Preprints (www.preprints.org) | NOT PEER-REVIEWED | Posted: 4 October 2018 doi:10.20944/preprints201810.0071.v1

The factor can vary from 0 to 1. The simply-supported or fully clamped condition will be the limiting case with the value of 0 or 1, respectively. This range of values from 0 to 1 provides engineers an intuitive manner for the extent of fixity available in a connection [12]. Moreover, this factor is insensitive to R, and a simple linear model will produce satisfactory results for design practice [13]. Therefore, the fixity factor in Eq. (1) is introduced to the floor-to-wall connections in CLT buildings in the present study.

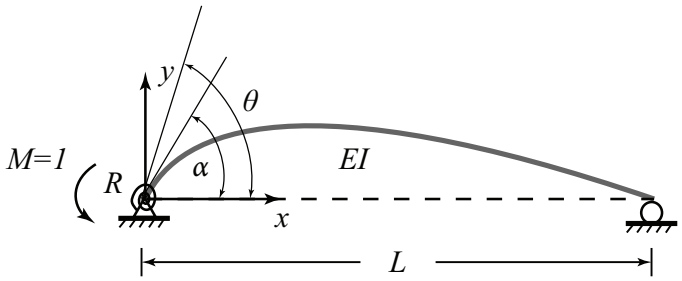

Figure 1. Definition of the end-fixity factor

3. Analytical methods

3.1. Rotational restraint coefficients

In order to consider the influence of rotational restraints, design coefficients can be developed for calculating the fundamental frequency and deflection of restrained beams through multiplying corresponding values of simply supported beams. In this manner, the fundamental natural frequency of a rotationally restrained beam can be expressed as

$$f = C_f \frac{\pi}{2L^2}\sqrt{\frac{EI}{\rho A}} \tag{3}$$

where C_f is the rotational restraint coefficient for the fundamental frequency, L, EI, ρ and A are the span, flexural rigidity, density of beam, and cross sectional area, respectively. It should be noted that the part of $\frac{\pi}{2L^2}\sqrt{\frac{EI}{\rho A}}$ on the right-hand side of Eq. (3) is the fundamental frequency of a simply-supported beam. Similarly, the mid-span deflection, d, of a rotational restrained beam under a point load is given by

$$d = C_d \frac{PL^3}{48EI} \tag{4}$$

in which C_d is the rotational restraint coefficient for deflection. Subsequently, the analytical expressions of proposed restraint coefficients, C_f and C_d, are derived in the following sections.

3.2. Fundamental frequency of rotationally restrained beams

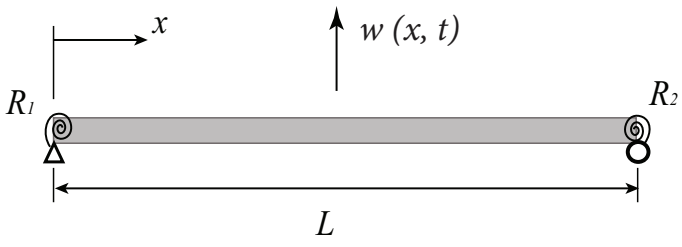

Figure 2. Rotationally restrained beam

Preprints (www.preprints.org) | NOT PEER-REVIEWED | Posted: 4 October 2018 doi:10.20944/preprints201810.0071.v1

A rotationally restrained beam with rotational stiffness R_1 and R_2 at the two ends is shown in Fig. 2. The rotational restraints are assumed to be proportional to the end rotations and the restraint stiffness, R_1 and R_2, may have any value in the range between simply supported (i.e., zero) and completely restrained (i.e., infinity). The corresponding rotational end-fixity factors can be determined by

$$r_1 = \frac{1}{1+3\dfrac{EI}{R_1 L}} \quad \text{and} \quad r_2 = \frac{1}{1+3\dfrac{EI}{R_2 L}} \tag{5}$$

For beam with complex boundary conditions as shown in Fig. 2, the finite Fourier Sine transform [15] can be applied to obtain exact series solutions of free vibration. Upon assuming harmonic motion for the free vibration analysis, the displacement $w(x,t)$ can be expressed as

$$w\left(x,\ t\right) = \psi\left(x\right)\cos\omega t \tag{6}$$

where ω is the natural circular frequency and $\psi(x)$ is the modal displacement function. Then, the governing equation can be expressed by [16]

$$EI\frac{d^4\psi\left(x\right)}{dx^4} - \rho A\omega^2\psi\left(x\right) = 0 \tag{7}$$

The boundary conditions of the beam can be expressed as

$$\psi = 0,\ \ R_1\frac{d\psi}{dx} = EI\frac{d^2\psi}{dx^2} \quad at\ x = 0 \tag{8a}$$

$$\psi = 0,\ \ R_2\frac{d\psi}{dx} = -EI\frac{d^2\psi}{dx^2} \quad at\ x = L \tag{8b}$$

To solve Eq. (7), the pair of the finite sine transform for $\psi(x)$ is defined as

$$\bar{\psi}(m) = \int_0^L \psi(x)\sin\alpha_m x dx \tag{9a}$$

$$\psi(x) = \frac{2}{L}\sum_{m=1}^{\infty}\bar{\psi}(m)\sin\alpha_m x \tag{9b}$$

where

$$\alpha_m = \frac{m\pi}{L}\ (m = 1,2,3,...) \tag{10}$$

The complete solving procedure can be found in [17]. At last, the characteristic function was produced as

$$m^4\bar{\psi}(m) + \frac{6m}{\pi^2}\sum_{i=1}^{\infty}\left[\frac{r_1}{1-r_1} + (-1)^{i+m}\frac{r_2}{1-r_2}\right] i\bar{\psi}(i) - \lambda^4\bar{\psi}(m) = 0 \tag{11}$$

where

$$\lambda^4 = \frac{\rho AL^4}{EI\pi^4}\omega^2 \tag{12}$$

The matrix form of Eq. (11) is given by

$$\mathbf{A\Psi} = \lambda^4\mathbf{\Psi} \tag{13}$$

Preprints (www.preprints.org) | NOT PEER-REVIEWED | Posted: 4 October 2018 doi:10.20944/preprints201810.0071.v1

where $\mathbf{\Psi} = [\bar{\psi}(1), \bar{\psi}(2), \ldots, \bar{\psi}(M)]$, if only the first M vibration modes of the beam are considered and $\mathbf{A}$ is the corresponding coefficient matrix of size $M \times M$ whose elements can be expressed as

$$A_{ii} = i^4 + \frac{6i^2}{\pi^2}\left[\frac{r_1}{1-r_1} + \frac{r_2}{1-r_2}\right] \tag{14a}$$

$$A_{ij} = \frac{2ij}{\pi^2}\left[\frac{r_1}{1-r_1} + (-1)^{i+j}\frac{r_2}{1-r_2}\right] \tag{14b}$$

in which $i = 1, 2, \ldots, M$, $j = 1, 2, \ldots, M$ but $i \neq j$.

The frequency parameter λ can be obtained by solving the eigenvalue problem of Eq. (13). After that, by using the first value of λ and rearranging Eq. (12), the fundamental natural frequency of the rotationally restrained beam can be expressed as

$$f = \lambda_1^2 \frac{\pi}{2L^2}\sqrt{\frac{EI}{\rho A}} \tag{15}$$

in which λ_1 is the first value of λ. As a result, the restraint coefficient of the fundamental frequency will be determined by

$$C_f = \lambda_1^2 \tag{16}$$

Although the foregoing procedure for determining C_f is straightforward and simple, it is also desirable to develop a simplified formula describing the relationship between the rotational fixity factors and their corresponding coefficient of C_f for engineering practice. For simplicity, restraints at the two ends are assumed to be equal. Then, the coefficient C_f for different rotational fixity factors ranging from 0 to 1 was obtained by solving the eigenvalue problems of Eq. (13) with truncating the infinite series solutions at $M = 1000$. In attempting to derive simplified formulas, the polynomial curve fitting technique was adopted and the coefficients can be conveniently approximated by

$$C_f = 0.85r^3 - 0.3r^2 + 0.71r + 1 \tag{17}$$

The simplified formula of Eq. (17) generated the coefficient of determination $R^2 = 0.9999$, which indicates that the simplified formula have excellent agreements with numerical results. Furthermore, coefficient values obtained by Eq. (17) and corresponding numerical results are compared as shown in Fig. 3. It can be observed that C_f increase with an increase in the fixity factor from 1 (simply supported) to 2.26 (fully clamped).

Preprints (www.preprints.org) | NOT PEER-REVIEWED | Posted: 4 October 2018 doi:10.20944/preprints201810.0071.v1

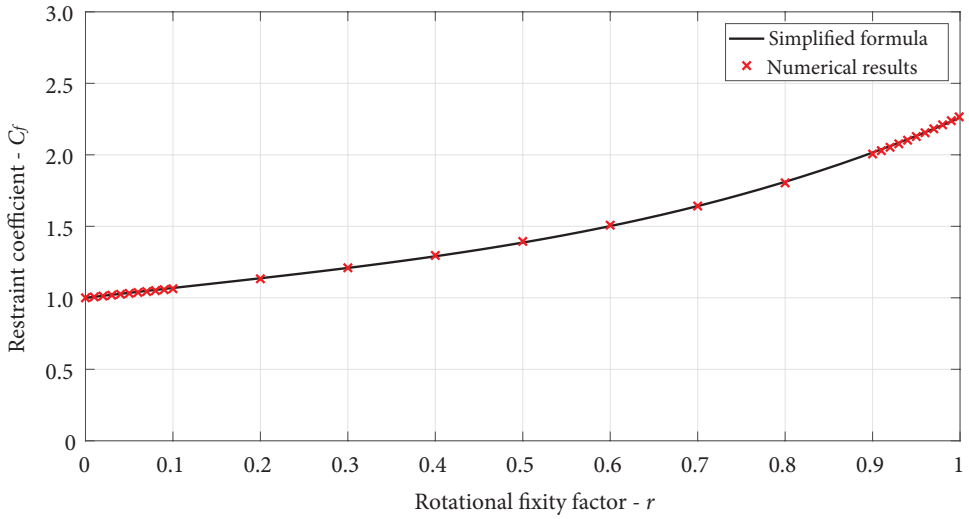

Figure 3. Comparison of C_f between numerical results and predictions by using the simplified formula

3.3. Deflection under a point load

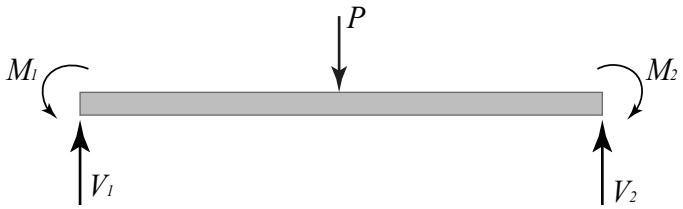

Figure 4. Free body diagram of a rotationally restrained beam

For a rotationally restrained beam under a concentrated load at the center as shown in Fig. 4, the corresponding end moments can be expressed as [13]

$$M_1 = \frac{3}{8}\frac{r_1(2-r_2)}{4-r_1r_2}PL \tag{18a}$$

$$M_2 = \frac{3}{8}\frac{r_2(2-r_1)}{4-r_1r_2}PL \tag{18b}$$

By using the end moments of Eq. (18), the mid-span deflection can be given by

$$y_{max} = \frac{PL^3}{48EI} - \frac{L^2}{16EI}(M_1 + M_2) \tag{19}$$

Substituting M_1 and M_2 in Eq. (18) into Eq. (19) yields

$$y_{max} = \frac{5r_1r_2 - 9(r_1+r_2) + 16}{16 - 4r_1r_2}\frac{PL^3}{48EI} \tag{20}$$

In particular, if the beam ends have the same rotational restraints ($r = r_1 = r_2$), the deflection y_{max} in Eq. (19) can be simplified to

$$y_{max} = \frac{5r^2 - 18r + 16}{16 - 4r^2}\frac{PL^3}{48EI} \tag{21}$$

Preprints (www.preprints.org) | NOT PEER-REVIEWED | Posted: 4 October 2018 doi:10.20944/preprints201810.0071.v1

Thus, the restraint coefficient for deflection in Eq. (4), C_d, can be expressed as

$$C_d = \frac{5r^2 - 18r + 16}{16 - 4r^2} \tag{22}$$

For the limiting cases,

$$y_{max} = \begin{cases} \dfrac{PL^3}{48EI}, & r = 0 \text{ and } C_d = 1 \text{ for simple end} \\ \dfrac{PL^3}{192EI}, & r = 1 \text{ and } C_d = \frac{1}{4} \text{ for fully-clamped end} \end{cases} \tag{23}$$

In summary, the relationship between the restraint coefficient C_d and the rotational fixity factor r is illustrated in Fig. 5. It can be found that C_d varies in a range from 0.25 to 1 and decreases with any increase in the end-fixity factor. Furthermore, Eq. (22) can be inversely applied to determine the end-fixity factor after measuring the mid-span deflections of the simply-supported beam and restrained beam.

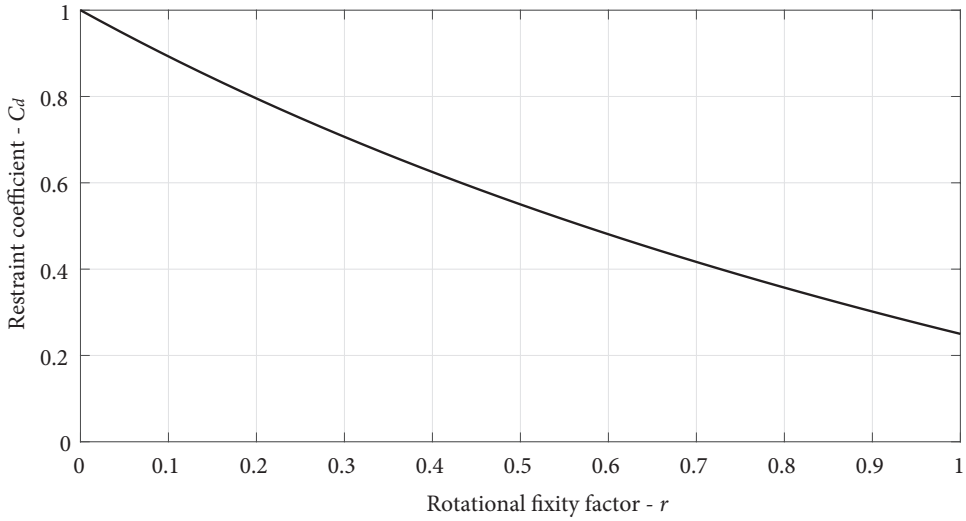

Figure 5. Relationship between the restraint coefficient C_d and the rotational fixity factor r

4. Validation studies

In this section, the proposed analytical approach was validated by using previous test results. At first, the restraint coefficient of C_d was calculated by using the mid-span deflection of a restrained beam divided by that of the reference simply-supported beam. After that, the end-fixity factor was determined based on Eq. (22). Then, the restraint coefficient C_f for the fundamental frequency was obtained by substituting the factor value into Eq. (17). Consequently, the fundamental natural frequency for each CLT panel with different restraints was calculated and compared with test results.

4.1. Previous experimental study

Previous experimental study was conducted by Hernández and Chui [18] to investigate the vibration performance of a 1 meter wide 3-ply CLT panel (0.079 m depth) supported on two sides with the three different end supports as shown in Fig. 6: (a) top load over two support edges (loaded support), (b) direct fastening to support using self-tapping screws (screwed support), and (c) ledger support. During the tests, the rotational stiffness of the different end supports was altered by increasing the magnitude of the applied load, number of the screws fastening the panel ends, and number of screws on the ledgers, respectively. Details of end-support configurations are shown in Table 1 for

Preprints (www.preprints.org) | NOT PEER-REVIEWED | Posted: 4 October 2018 doi:10.20944/preprints201810.0071.v1

completeness. Five different spans (i.e., 4.5 m, 4.1 m, 3.7 m, 3.3 m, and 2.9 m) were created by sequentially cutting the CLT strips at a interval of 0.4 m. In addition, the simply-supported condition was also tested for reference.

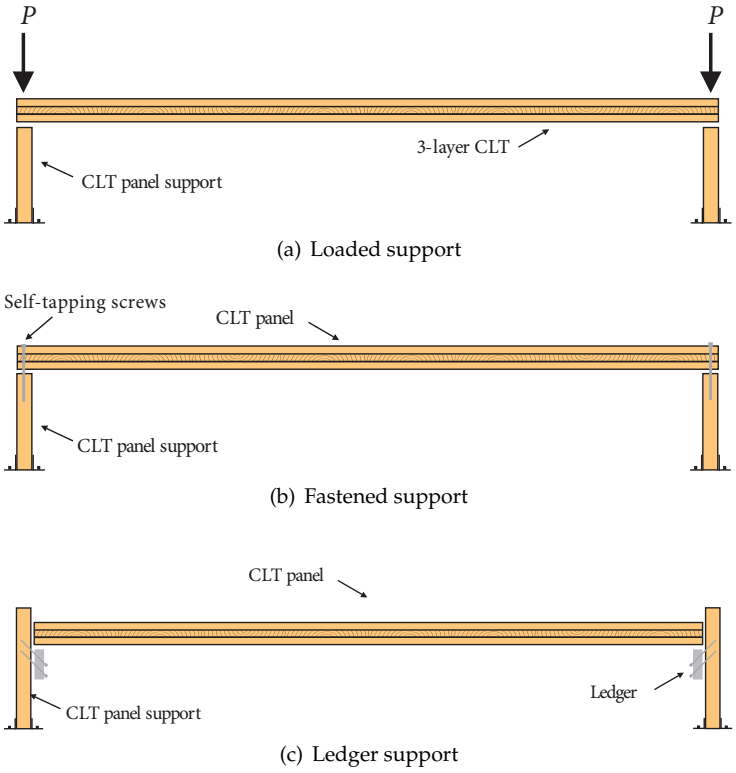

Figure 6. Three end support setups: (a) loads applied over the end supports, (b) panel ends fastened to supports by self-tapping screws, and (c) panel ends supported by a ledger below and fastened to the ledger with three screws. (adapted from [18])

Table 1. Details of end support configurations in tests

End support configurations	Label	Descriptions
Simply supported	SS	No restraints
Load	P10	5 kN at each support
	P20	10 kN at each support
	P40	20 kN at each support
	P60	30 kN at each support
Screws	S1	1 screws at the center of each support
	S2	3 screws on each support
	S3	5 screws on each support
	S4	9 screws on each support
	S5	13 screws on each support
Ledger	L1	4 screws on each ledger
	L2	6 screws on each ledger
	L3	10 screws on each ledger
	L4	14 screws on each ledger
	L5	18 screws on each ledger

4.2. End-fixity factors

Since the mid-span deflection has been measured for the reference simply-supported CLT panels and those panels with different restrained end-supports, the end-fixity factors can be inversely

Preprints (www.preprints.org) | NOT PEER-REVIEWED | Posted: 4 October 2018 doi:10.20944/preprints201810.0071.v1

determined by using Eq. (4) and (22) for each specific end support. The fixity factors obtained by such inverse method are tabulated in Table 2. Since the ledger support has been found with a minimal effect on the rotational stiffness, only loaded supports and screwed supports are investigated herein.

Table 2. Rotational fixity factors r determined by using test results of mid-span deflections

End support c | configuration	Labels	Span (m)				
		4.5	4.1	3.7	3.3	2.9
Loaded	P10	0.12	0.17	0.11	0.15	0.16
	P20	0.18	0.24	0.18	0.26	0.21
	P40	0.34	0.33	0.28	0.33	0.32
	P60	0.36	0.39	0.32	0.36	0.38
Screwed	S1	0.07	0.13	0.04	0.11	0.08
	S2	0.13	0.18	0.13	0.18	0.16
	S3	0.19	0.24	0.19	0.23	0.20
	S4	0.25	0.32	0.30	0.27	0.30
	S5	0.30	0.39	0.32	0.30	0.37

4.3. Comparisons of the fundamental frequency

In this section, the test results of the fundamental frequency were used to validate the proposed analytical methods. At first, the rotational restraint coefficients C_f were determined based on the fixity factors in Table 2. Then, the fundamental frequency was predicted based on Eq. (3) and compared with the corresponding test results in [18]. Comparisons between test results and predictions of the fundamental natural frequency for different end supports are tabulated in Table 3 and 4. Excellent agreements can be found between the test results and predictions. For illustration purpose, the percentage difference for loaded support specimens are illustrated in Fig. 7.

Table 3. Comparisons between tested results and predictions of the fundamental frequency for loaded support specimens

End support configurations	Item	Span (m)				
		4.5	4.1	3.7	3.3	2.9
SS	f_t (Hz)	8.88	10.63	13.13	15.88	19.50
P10	f_t (Hz)	10.50	12.00	14.50	18.38	23.38
	C_f	1.08	1.11	1.07	1.10	1.11
	f_p (Hz)	9.63	11.85	14.10	17.52	21.67
	%	-8.26	-1.29	-2.75	-4.66	-7.30
P20	f_t (Hz)	11.00	12.63	15.25	19.38	24.63
	C_f	1.12	1.16	1.12	1.18	1.14
	f_p (Hz)	9.94	12.37	14.75	18.74	22.31
	%	-9.61	-2.06	-3.26	-3.33	-9.42
P40	f_t (Hz)	11.75	13.63	16.38	20.38	26.13
	C_f	1.24	1.23	1.19	1.23	1.23
	f_p (Hz)	11.03	13.11	15.69	19.53	23.91
	%	-6.15	-3.85	-4.21	-4.15	-8.48
P60	f_t (Hz)	12.13	14.13	17.00	21.25	27.13
	C_f	1.25	1.28	1.22	1.25	1.27
	f_p (Hz)	11.13	13.59	16.08	19.93	24.78
	%	-8.28	-3.79	-5.39	-6.22	-8.65

Note: f_t test results of the fundamental frequency
C_f rotational restraint coefficient for frequency
f_p predictions of the fundamental frequency
% difference between f_t and f_p in percentage

Preprints (www.preprints.org) | NOT PEER-REVIEWED | Posted: 4 October 2018 doi:10.20944/preprints201810.0071.v1

Table 4. Comparisons between tested results and predictions of the fundamental frequency for screwed support specimens

End support configurations	Item	Span (m)				
		4.5	4.1	3.7	3.3	2.9
SS	$f_t(Hz)$	8.88	10.63	13.13	15.88	19.50
S1	$f_t(Hz)$	9.38	11.63	13.50	16.75	21.25
	C_f	1.05	1.09	1.03	1.08	1.06
	f_p (Hz)	9.31	11.59	13.53	17.11	20.61
	%	-0.79	-0.36	0.21	2.16	-2.99
S2	f_t (Hz)	10.38	12.13	14.38	18.13	23.00
	C_f	1.09	1.12	1.09	1.13	1.11
	f_p (Hz)	9.70	11.95	14.27	17.88	21.67
	%	-6.55	-1.47	-0.77	-1.37	-5.76
S3	f_t (Hz)	11.00	12.75	15.38	18.88	23.75
	C_f	1.13	1.17	1.13	1.16	1.14
	f_p (Hz)	10.01	12.40	14.84	18.41	22.18
	%	-8.96	-2.75	-3.48	-2.48	-6.61
S4	f_t (Hz)	11.75	13.38	16.38	19.88	24.63
	C_f	1.17	1.22	1.21	1.19	1.21
	f_p (Hz)	10.41	13.00	15.85	18.82	23.59
	%	-11.38	-2.83	-3.21	-5.34	-4.20
S5	f_t (Hz)	12.25	13.75	16.75	20.25	25.25
	C_f	1.208059	1.28268	1.22051	1.21253	1.261511
	f_p (Hz)	10.73	13.63	16.03	19.25	24.60
	%	-12.43	-0.84	-4.33	-4.91	-2.58

Note: f_t test results of the fundamental frequency
C_f rotational restraint coefficient for frequency
f_p predictions of the fundamental frequency
% difference between f_t and f_p in percentage

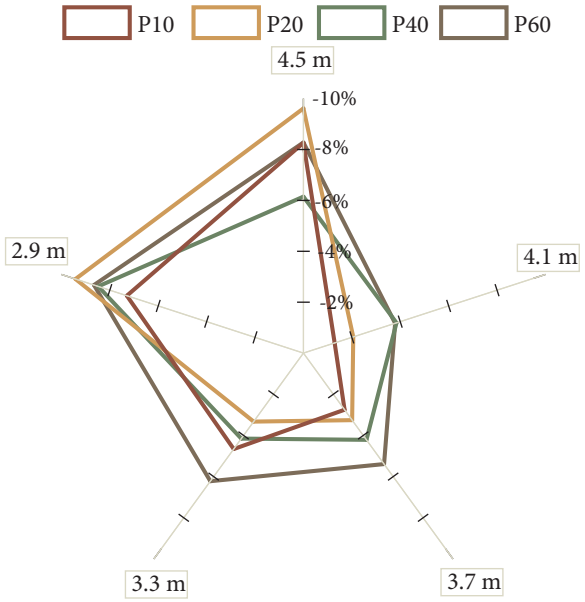

Figure 7. Percentage difference between tested results and predictions of the fundamental frequency of loaded support specimens

5. Conclusions

In the present paper, an analytical treatment has been conducted for CLT panels with various end fixities by introducing the end-fixity factor. The analytical expressions for the fundamental natural frequency and the mid-span deflection under a concentrated load were derived and associated rotational restraint coefficients defined for the design of vibration serviceability of CLT floors. A simplified formula of the restraint coefficient for the fundamental frequency was developed by using curve-fitting to assist engineers in practical design. At last, the predicted results by using the proposed analytical methods are compared with test results of the fundamental frequency and excellent agreement is obtained. It can be concluded that the proposed end fixity factor and derived formulas for restraint coefficients can be recommended as an effective mechanics-based approach to account for the effect of end support conditions of CLT floors and optimize the design of the floors with acceptable vibration performance.

Conflicts of Interest: The funding sponsors had no role in the design of the study; in the collection, analyses, or interpretation of data; in the writing of the manuscript, and in the decision to publish the results.

References

1. Karacabeyli, E.; Douglas, B. *Cross-Laminated Timber (CLT) Handbook*, U.S. ed.; FPInnovations: Pointe-Claire, QC, Canada, 2013.
2. Gsell, D.; Feltrin, G.; Schubert, S.; Steiger, R.; Motavalli, M. Cross-laminated timber plates: Evaluation and verification of homogenized elastic properties. *Journal of structural engineering* **2007**, *133*, 132–138.
3. Chúláin, C.U.; Sikora, K.; Harte, A.M. Influence of connection systems on serviceability response of CLT timber flooring. The Proceedings of 2016 World Conference on Timber Engineering WCTE; , 2016.
4. Jarnerö, K.; Brandt, A.; Olsson, A. Vibration properties of a timber floor assessed in laboratory and during construction. *Engineering structures* **2015**, *82*, 44–54.
5. Zimmer, S.; Augustin, M. Vibrational behaviour of cross laminated timber floors in residential buildings. The Proceedings of 2016 World Conference on Timber Engineering WCTE; , 2016.
6. Hamm, P.; Richter, A.; Winter, S. Floor vibrations – new results. The Proceedings of 2010 World Conference on Timber Engineering WCTE, 2012, pp. 269–275.
7. Hu, L.; Gagnon, S. Controlling cross-lamminated timber (CLT) floor vibrations: fundamentas and method. The Proceedings of 2012 World Conference on Timber Engineering WCTE, 2012, pp. 269–275.
8. CSA O86-14. *Engineering Design in Wood*; Canadian Standard Association, 2014.
9. Schultz, J.A.; Johnson, B. Evaluation of North American vibration standards for mass-timber floors. Dynamics of Coupled Structures, Volume 1. Springer, 2014, pp. 253–259.
10. Bapat, A.V.; Venkatramani, N.; Suryanarayan, S. Simulation of classical edge conditions by finite elastic restraints in the vibration analysis of plates. *Journal of Sound and Vibration* **1988**, *120*, 127–140.
11. Zhang, S.; Xu, L. Bending of rectangular orthotropic thin plates with rotationally restrained edges: A finite integral transform solution. *Applied Mathematical Modelling* **2017**, *46*, 48–62.
12. Cunnigham, R. Some aspects of semi-rigid connections in structural steelwork. *The Structural Engineer* **1990**, *68*, 85–92.
13. Xu, L. Second-order analysis for semirigid steel frame design. *Canadian Journal of Civil Engineering* **2001**, *28*, 59–76.
14. Monforton, G.; Wu, T.H. Matrix analysis of semi-rigid connected frames. *Journal of the Structural Division* **1963**, *89*, 13–24.
15. Zhang, S.; Xu, L.; Li, R. New exact series solutions for transverse vibration of rotationally-restrained orthotropic plates. *Applied Mathematical Modelling* **2019**, *65*, 348–360.
16. Humar, J. *Dynamics of structures*, 2 ed.; CRC Press, 2002.
17. Zhang, S.; Xu, L. Determination of equivalent rigidities of cold-formed steel floor systems for vibration analysis, Part I: Theory. *Thin-Walled Structures* **2018**, *132*, 25–35.
18. Hernández, S.A.M.; Chui, Y.H. Effect of end support conditions on the vibrational performance of cross-laminated timber floors. The Proceedings of 2014 World Conference on Timber Engineering (WCTE); , 2014.